Use of sludge produced from reject brine as a supplementary cementitious material with enhanced carbonation capability

(article starts on next page)

Use of sludge produced from reject brine as a supplementary cementitious material with enhanced carbonation capability

Tangwei Mi [a], Yongqiang Li [b], En-Hua Yang [a], Cise Unluer [c,*]

[a] *School of Civil and Environmental Engineering, Nanyang Technological University, 50 Nanyang Avenue, 639798, Singapore*
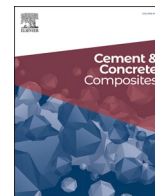[b] *Division of Building Technology, Chalmers University of Technology, 41296, Gothenburg, Sweden*
[c] *Department of Civil Engineering and Management, University of Manchester, M13 9PL, Manchester, United Kingdom*

ARTICLE INFO

ABSTRACT

Sludge obtained from reject brine via a novel two-step approach involving precipitation and filtration was used as a supplementary material in reactive magnesia cement (RMC) and Portland cement (PC) mixes. Detailed evaluation of the performance and microstructure of the resultant cement pastes revealed the underlying mechanism. Incorporating 25 % (of the binder content) sludge in RMC mixes significantly increased the compressive strength under ambient and carbonation-based curing, which was more than doubled under the latter condition. While the strength of PC mixes decreased with the use of sludge, it still exceeded 30 MPa under carbonation. Increase in hydration heat observed in sludge-containing mixes was attributed to the presence of brucite acting as nucleation sites. ~30 % reduction in CO_2 emissions and ~25 % reduction in energy consumption was achieved by simply incorporating sludge in the designed mixes. Furthermore, sludge enhanced carbonation in RMC and PC mixes by increasing the amount of CO_2 sequestered at 28 days by 25.9 % and 41.1 %, respectively. Overall, the feasibility of re-purposing reject brine by directly using the produced sludge was demonstrated, offering a sustainable alternative for concrete production with a significantly reduced environmental impact.

1. Introduction

Reactive magnesia cement (RMC) is attracting increasing attention as an alternative cementitious material to Portland cement (PC) in an attempt to reduce the overall CO_2 emissions associated with cement production and use [1]. RMC can be produced via 2 main methods, namely the dry route and the wet route [2]. In dry route, RMC is derived through the calcination of magnesite within the temperature range of 700–1000 °C. Notably, the calcination temperature in this process is significantly lower than that employed in PC production (~1450 °C) [3]. Alternatively, the wet route involves the extraction of RMC from seawater or reject brine that contains elevated concentrations of magnesium (Mg) [4]. Within this approach, the Mg-bearing product is initially precipitated via the use of an alkali base to produce magnesium hydroxide (Mg(OH)$_2$), which then undergoes washing and calcination at a comparatively low temperature to yield the final product, RMC [5,6].

While both the dry and wet routes have demonstrated feasibility and potential for commercialization, certain limitations persist. In the dry

route, the calcination process can lead to around 1 ton of CO_2 emissions to produce 1 ton of RMC [7]. The overall CO_2 emissions from the dry route are therefore comparable to those of PC production [7], though RMC is capable of sequestering some of this CO_2 during curing, resulting in strength development [8]. In the wet route, benefiting from the absence of magnesite calcination, CO_2 emissions are significantly reduced. Moreover, RMC produced through the wet route typically exhibits higher purity and reactivity [2]. One of the main materials used during this process for the source of Mg, reject brine, is a by-product of desalination process, and is commonly disposed of by being poured back into the seawater in marine areas or over the land surface in inland areas, posing a threat to local ecosystems [9]. With increasing global demand for clean water and the critical role that desalination water plays as a water supply, the production of reject brine has reached ~141.5 million cubic meters per day [10]. Consequently, the utilization of reject brine for RMC production through the wet route emerges as a promising practice. This approach not only addresses the challenges associated with the disposal and management of reject brine, but also
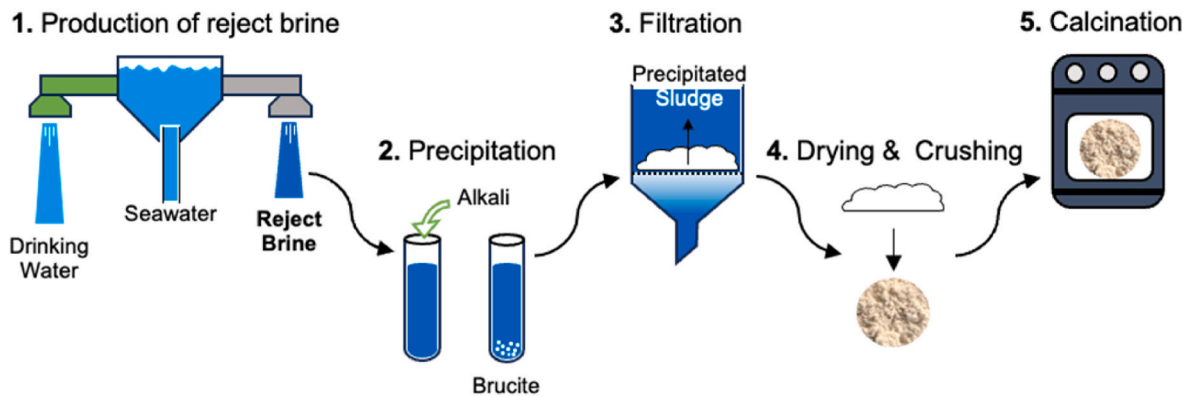

Fig. 1. Procedure of the synthesis of RMC from reject brine [2,13].

contributes to meeting the demand for alternative cementitious materials.

The production of RMC via the wet route is a multi-step process associated with CO_2 emissions originating primarily from the use of alkaline agents for precipitating magnesium ions as brucite, as well as from mechanical operations such as stirring, centrifugation, grinding, and calcination. Among these, the choice of alkali plays a critical role in determining the overall carbon footprint. Common alkaline agents include CaO [11], NaOH [2] and NH_4OH [12], each resulting in varying levels of CO_2 emissions throughout the process. One recent study explored the environmental implications of different alkali types in RMC production [13]. Their findings suggested that CaO was the most environmentally favourable option when compared to NaOH, NH_4OH, and C_2H_7NO. Under optimal conditions, the use of CaO for producing 1 kg of RMC resulted in 1.94 kg of CO_2 emissions. In particular, the production process of RMC from reject brine normally involves a 5-step procedure, as illustrated in Fig. 1. Within this process, the primary contributors of CO_2 emissions are the embodied CO_2 in the alkali base. The second major source of CO_2 emissions are the energy-intensive steps 4 and 5, which account for approximately 87.81 % of the total CO_2 emissions of the entire procedure (excluding the embodied CO_2 in alkali) [13]. Therefore, further optimization of this production procedure is needed to improve its sustainability and enable its large-scale implementation in locations where desalination in highly adopted for clean water production.

Past efforts to improve the sustainability and efficiency of RMC production from reject brine include the optimization of the alkali type, encompassing both Ca- and Na-bearing compounds [11,14–17]. However, the utilization of Ca-bearing compounds has the drawback of Ca-based impurity precipitation in the produced RMC [6,11], whilst Na-bearing compounds are constrained by their relatively high cost, embodied energy and CO_2 emissions associated with their production. Consequently, the search for alternative and more sustainable alkali sources remains ongoing. Concurrently, advancements in the production procedure depicted in Fig. 1 have also focused on tailoring the calcination conditions, revealing that a minimal calcination energy of ~2.08 GJ can be achieved with a 2-h calcination at 500 °C [18].

Given the potential in minimizing the energy consumption during calcination, the feasibility of utilizing brucite directly without calcination was also explored [11]. Successful utilization of brucite was demonstrated by the attainment of a paste with a strength of around 30 MPa under carbonation curing, which was limited at 10 MPa under ambient curing [11]. By eliminating Step 5 from the production process, a substantial improvement in the overall sustainability and efficiency of production was realized. However, despite employing a water-to-brucite ratio of 0.6, the resulting paste exhibited limited moldability and workability in previous work [11]. To address this, additional compaction (i.e. with a pressure of 2.5 MPa at a rate of 0.5 mm/min for 1 min) was employed to cast the brucite into compacted pellets,

potentially limiting its practical application on a large scale.

Concrete sludge, a prevalent waste generated by ready-mix concrete plants, has conventionally been repurposed as fine or coarse aggregates [19,20] or a cementitious material through energy-intensive and time-consuming drying and grinding processes [21,22]. In response to the resource-intensive nature of these methods, an innovative approach has been proposed for the recycling and reuse of concrete sludge [23]. Particularly, considering the residual cementitious content of concrete sludge, a novel concrete mix was fabricated by directly blending PC with concrete sludge. Similar to concrete sludge, the sludge precipitated at Step 3 in Fig. 1 has a high water-to-solid ratio, which would normally require drying and grinding for reuse. The direct reuse of this precipitated sludge can be facilitated via its incorporation in RMC/PC mixes. The benefits of using precipitated sludge include: (i) elimination of energy consumption during Steps 4 and 5, (ii) reduction in the overall production duration, and (iii) conservation of water required for the preparation of new paste/concrete mixes.

Based on these advantages, coupled with the benefits of recycling and reuse of reject brine, this study explored the feasibility of a two-step method (i.e. involving precipitation and filtration), to enable the direct utilization of precipitated sludge as a cement replacement. PC- and RMC-based mixes involving the sludge were prepared and analyzed for their reaction mechanisms, mechanical performance and microstructural development. Furthermore, the carbonation of the resulting mixes was assessed through thermogravimetric analysis, x-ray diffraction and Raman spectroscopy. Finally, a sustainability analysis was undertaken to reveal the environmental impact of the developed mixes. The results of this work are aimed to contribute to the development of a sustainable methodology for the recycling and reuse of reject brine and other by-products (sludge) emerging during the production of cement through the wet route.

2. Materials and methodology

2.1. Materials

RMC was purchased from Lingshou Minerals Processing Plant in China, and PC was sourced from Lafarge Cement Pte. Ltd. The sludge was initially prepared from reject brine by adhering to the Step 1 to Step 3 as depicted in Fig. 1. Through preliminary tests, the water-to-brucite ratio was determined to be 2.03 ± 0.07. Given the constrained quantity of sludge and the slight variation in the water-to-solid ratio across different batches, the sludge utilized in this study was prepared via a standardized procedure. Specifically, brucite and water were combined at a mass ratio of 2:1 in a plastic container, which was then subjected to continuous homogenization for 24 h using an orbital shaker to ensure the complete blending of the components.

Table 1

Mix proportion of the paste samples prepared in this study.

Mixes	Sludge	RMC	PC	Water
RMC + S	12	12	0	0
RMC	0	16	0	8
PC + S	12	0	12	0
PC	0	0	16	8

Table 2

LF-NMR test parameters.

Pulse sequence	Spectrometer frequency (MHz)	Sampling bandwidth (kHz)	180° Pulse Width (μs)	Waiting time (ms)	Number of scans
CPMG	12	200	10.8	1500	16

2.2. Sample preparation

Four mixes were designed, labelled as RMC + S, RMC, PC + S, and PC, each with specific mix proportions as detailed in Table 1. For each mix design, all materials were thoroughly mixed and cast into 10 mm cube moulds. The moulds were tamped to eliminate most voids within the mixture. After curing for 24 h, the cube samples were demoulded and subsequently subjected to carbonation (30 °C, 80 % relative humidity (RH) and 20 % CO_2 concentration) and ambient curing (30 °C, 80 % RH and 0.04 % CO_2 concentration). These samples were prepared to facilitate the assessment of compressive strength and pore size distribution. Following each compressive strength test, the specimens were collected and subsequently ground into fine powders for additional microscale measurements.

2.3. Compressive strength

The compression tests were conducted at 3d, 7d and 28d utilizing a Toni Technik Baustoffprüfsysteme machine operating under load control mode, with a testing rate set at 1 kN/min. Each test involved the preparation of three samples, and the reported values represent the average, accompanied by the standard deviation.

2.4. Isothermal calorimetry

Isothermal calorimetry was performed by using an I-Cal 8000 high precision calorimeter. The hydration heat of the four mixes was assessed, with a total of 24 g of material employed in each mix. The sludge, PC, RMC and water underwent a preheating process at 30 °C for 24 h to ensure uniform initial temperatures across all materials. Subsequently, the mixes were cast for approximately 15 s and immediately placed into the calorimeter channel for analysis.

2.5. Pore size distribution

Pore size distribution was evaluated by Low-Field Nuclear Magnetic Resonance (LF-NMR), a technique known for its exceptionally broad measurable ranges compared to other methods [24]. LF-NMR T_2 relaxation curves were acquired using a low-field NMR instrument (Meso-MR12-060H-I, Niumag, Suzhou, China) with specific parameters: input voltage of 220 V, 50/60 Hz, magnetic field strength of 0.3 ± 0.05 T, and power of 1000 W. The cubic samples, after 28 days of curing, were immersed in deionized water in a vacuum saturation device for one day to achieve a fully saturated condition. The detailed test parameters were outlined in Table 2, and the obtained results were all normalized per gram of the sample for comparison. Additionally, the transverse relaxation time (T_2) of porous media can be considered proportional to the surface-to-volume ratio (S/V) of the pores, as expressed in Equation (1) [25,26]:

$$\frac{1}{T_{2i}} = \rho_2 \frac{S_i}{V_i} = \frac{\lambda}{T_{2s}} \frac{S_i}{V_i} \tag{1}$$

where λ represents the thickness of the water layer (m); T_{2s} and T_{2i} denote the transverse relaxation time of the porous medium surface and the fluid, respectively (s); ρ_2 is the transverse relaxation rate; S_i is the pore surface area (μm^2), and V_i is the volume of the sample (μm^3).

2.6. Thermogravimetric analysis (TGA)

The CO_2 sequestration capability of different mixes was evaluated by TGA. A PerkinElmer TGA 4000 was employed in present work. The measurement was conducted within a temperature range between 30 °C
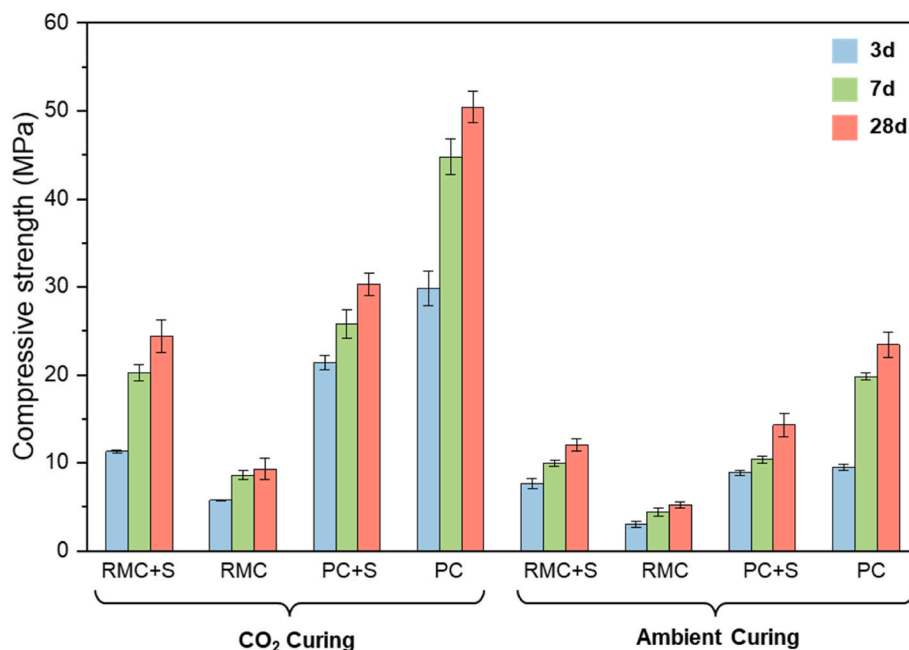

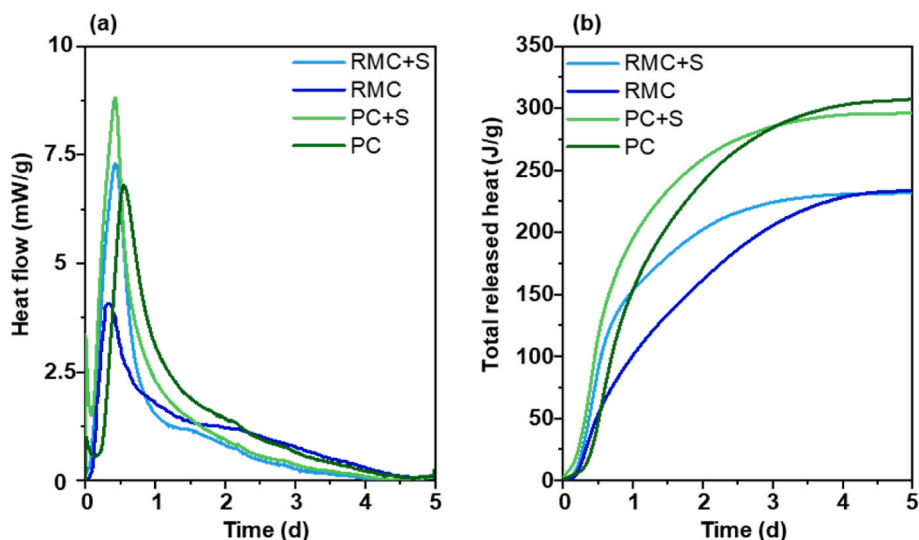**Fig. 2.** Compressive strength of RMC and PC mixes at 3, 7 and 28 days.

Fig. 3. Isothermal calorimetry results, showing: (a) heat flow and (b) total released heat.

and 900 °C, employing a heating rate of 10 °C/min and a flow rate of 20 mL/min under a nitrogen (N_2) atmosphere. Additionally, Differential Thermogravimetry (DTG) curves were also obtained to determine the temperature range corresponding to the decomposition of different phases.

2.7. X-ray diffraction (XRD) analysis

XRD was performed with a Bruker D8 Advance spectrometer to characterise the chemical composition of the carbonated mixes. XRD patterns were acquired using Cu Kα radiation (40 kV, 40 mA) at a scanning rate of 0.04° 2θ/step, over a range from 10 to 50° 2θ.

2.8. Raman spectroscopy

Raman spectroscopy was performed employing a Renishaw inVia Raman spectrometer equipped with a 785 nm laser. A New-Port M-5 × microscope objective lens was employed for the laser focusing, with a spot size of ~4 μm and a laser power of ~6 mW. To evaluate the carbonation products, Raman mapping measurements were performed on the samples subjected to carbonation curing after 3 d, 7 d and 28 d. For each sample, measurements were conducted in three random square areas with a matrix of 5 × 5, covering a range of 800 × 800 μm. Consequently, 75 spectra were collected from each sample, and each spectrum was recorded with an exposure time of 5 s and 2 accumulation times. However, the Raman spectra obtained from the paste consistently exhibited a noisy background, which could affect the accuracy of quantitative analysis. To address this, the background of each spectrum was removed using the baseline correction function in OriginPro.

3. Results and discussion

3.1. Compressive strength

The compressive strength results of RMC and PC mixes were depicted in Fig. 2, elucidating the impact of incorporating sludge into RMC and PC on their corresponding strength development. Under carbonation curing, RMC + S exhibited higher strength than RMC across all durations, surpassing RMC by over twofold at 28 days. Alternatively, the introduction of sludge into PC exhibited an adverse effect on strength development. Despite an observed reduction rate of approximately 39.0 %, the strength of PC + S remained relatively high at 30.3 MPa, meeting relevant requirements for non-structural applications. In terms of the

strength results under ambient curing conditions, RMC exhibited notably low strength which was consistent with that reported in literature [27]. Such reduced strength could be attributed to the straightforward transformation from MgO to Mg(OH)$_2$, without forming a product with a densely packed structure like calcium silicates hydrates (CSH) gel [28]. Intriguingly, the inclusion of sludge in RMC led to a moderate increase in strength under ambient curing, comparable to that of RMC under carbonation curing, reaching approximately 11.0 MPa after 28 days. Regarding PC under ambient curing, a decline of 38.0 % in strength was noted in PC + S compared to PC. This diminished strength could be associated with the substitution of PC with sludge. Overall, the incorporation of sludge resulted in increased strength for RMC and decreased strength for PC under both carbonation and ambient curing conditions.

3.2. Hydration heat

The isothermal calorimetry results, presented in Fig. 3, provided insights into the hydration heat of different mixes. The heat generated during the hydration of RMC and PC manifested in distinct peaks in hydration as depicted in Fig. 3 (a).

In the case of RMC and RMC + S, a prominent peak emerged at ~10 h, attributed to the hydration of MgO to form Mg(OH)$_2$ [29]. Remarkably, the inclusion of sludge enhanced the slope of the heat flow curves and, notably, intensified the major peak. Specifically, the intensity of the major peak in RMC + S was approximately twice that of RMC. It was thus inferred that the brucite in the sludge acted as seeds, significantly increasing the initial hydration rate [30]. However, owing to the higher MgO content in the RMC mix, the total released heat of RMC + S gradually aligns with that of RMC at 5 days, as depicted in Fig. 3 (b).

The hydration flow for PC and PC + S exhibited an initial distinct endothermic peak shortly after mixing, indicative of the rapid initial hydration of C$_3$S and C$_3$A during the pre-induction period, followed by a dormant period [31]. After a few hours of dormancy, a major peak became apparent, associated with the primary hydration of C$_3$S to form CSH gel and portlandite [32]. Similar to the phenomenon in RMC, the incorporation of sludge led to a more intense major peak which shifted to left, indicating a higher hydration rate at early stage. Accordingly, the total released heat of PC + S was higher than that of PC mix initially, which can be linked to the higher early strength of PC + S mix than that of PC mix before 3d under ambient curing as illustrated in Fig. 3 (b). However, due to the higher PC content in the PC mix, the total hydration heat of PC exceeded that of PC + S as the incorporation of sludge
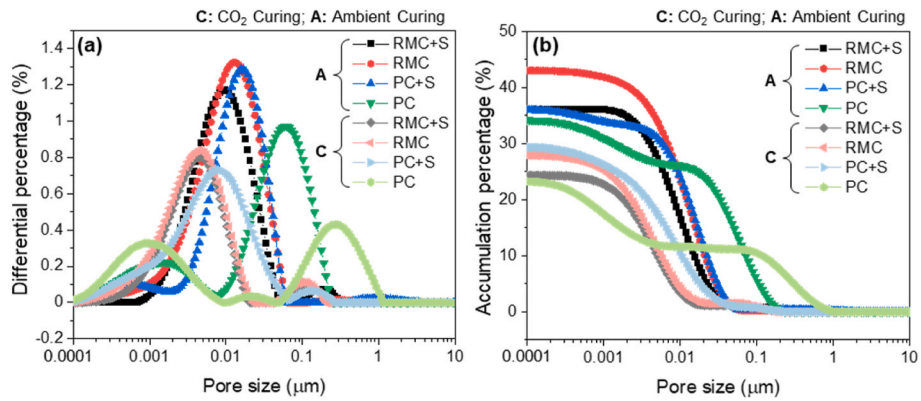
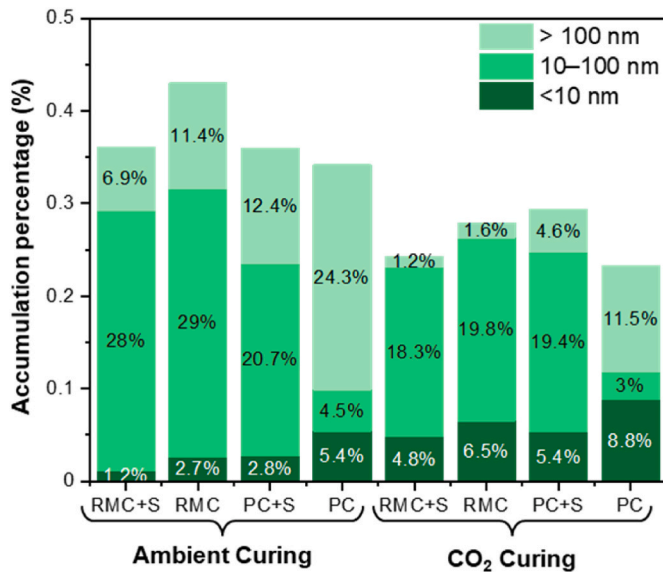**Fig. 4.** Pore size distribution of RMC and PC mixes after 28 days of curing.

Fig. 5. Different pore size contents of RMC and PC mixes.

Fig. 6. TGA and DTG curves of carbonated RMC and PC mixes after 28 days.

replaced 25 % of PC in the mix, a phenomenon potentially linked to the higher strength observed under ambient curing conditions [33].

Overall, the incorporation of sludge increased the hydration rate of both RMC and PC at the initial stage, which can be attributed to the existence of brucite in sludge acting as nucleation site in the mixes [34].

3.3. Pore size distribution

The pore size distributions of different mixes were measured using LF-NMR. Fig. 4 (a) depicted the pore size distribution of RMC and PC mixes, with the peaks indicating the most probable pore diameters [35]. Notably, the major peaks in PC + S, RMC and RMC + S mixes all shifted towards lower diameters in carbonated mixes when compared to those under ambient conditions. This observation revealed reductions in the major pore diameter of the cement pastes, consequently leading to densified microstructures. In PC mixes undergoing ambient curing, a major peak at around 60 nm and a minor peak at approximately 2 nm were observed, which transformed into two equally minor peaks after carbonation curing, indicating a reduction in macro pores.

Fig. 4 (b) presented the cumulative percentages of different mixes. Evidently, the mixes after ambient curing exhibited higher porosity than those after carbonation curing, which should be attributed to the formation of carbonated products that densify the microstructures of matrixes. Additionally, incorporating sludge in RMC and PC resulted in an increase and decrease in matrix porosity, respectively. This contrasting
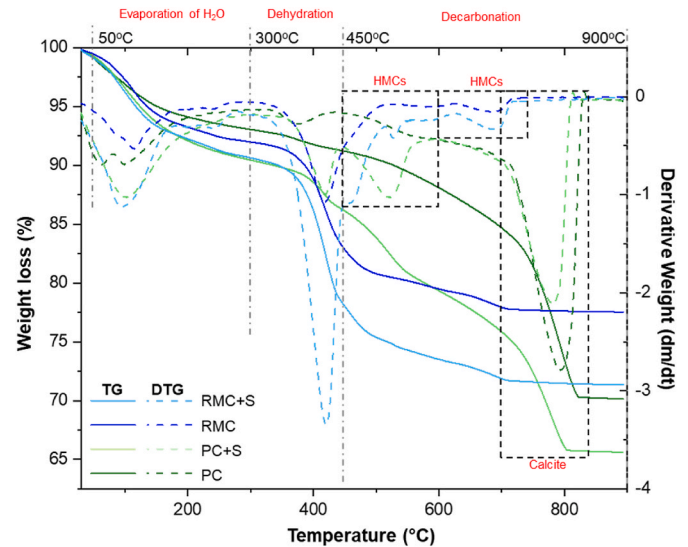
effect could be linked to the observed enhancement and reduction in the strength of RMC and PC mixes, respectively, as observed in present work. Notably, the highest porosity was observed in RMC after ambient curing, aligning with its lowest strength as illustrated in Fig. 2.

To further quantify the pore structures of the mixes, Fig. 5 presented the contents of different pore sizes for various mixes. The pores were categorized into gel pores (<10 nm), transition pores (10–100 nm), and large pores (>100 nm, including capillary and macro pores) [26,36,37]. Considering the impact of carbonation, a reduction in transition and large pores and an increase in gel pores were evident by comparing the carbonated mixes with the uncarbonated ones. This observation could be attributed to the formation of carbonation products that densify the pore structures of PC [38] and RMC matrixes [39], resulting in a transformation of large and transition pores into gel pores. Alternatively, the incorporation of sludge demonstrated inverse effects on RMC and PC. For RMC, the incorporation of sludge decreased the overall porosity of the matrixes under both ambient and carbonation curing, resulting in a higher compressive strength. On the other hand, the incorporation of sludge increased the overall porosity of the PC, especially for the content of capillary pores, which was corresponding to the lower compressive strength of PC + S mix than that of PC mix.

Overall, the outcomes derived from LF-NMR revealed a strong correlation between strength development and pore size distribution in different mixes.
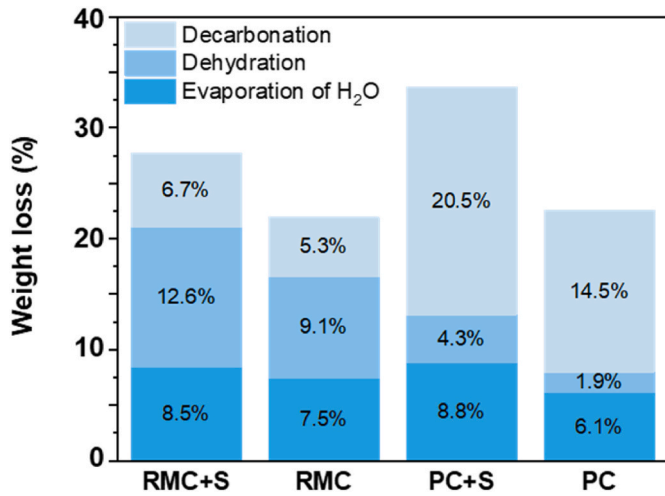
Fig. 7. Mass loss attributed to different decomposition stages in RMC and PC mixes.

3.4. Thermogravimetric analysis (TGA)

Fig. 6 showed the TGA and DTG curves of the mixes after carbonation curing for 28d. Multiple peaks were discernible in the DTG curve, corresponding to temperature ranges for different phase decompositions. Specifically, the weight loss in the range of 1) 50–300 °C was linked to the dehydration of water bonded to hydrated magnesium carbonates (HMCs) [40] or CSH and AFt [41], 2) 300–450 °C corresponded to the dehydration of $Mg(OH)_2$ [30,42,43] or $Ca(OH)_2$ [44], and 3) 450–900 °C was associated with the decarbonation of HMCs [40,45,46] or $CaCO_3$ [41]. The peaks over 500 °C were labelled as depicted in Fig. 6. Notably, a major peak at around 680 °C was observable in the DTG curves of both RMC + S and RMC mixes, with an additional peak at around 520 °C in the former mix, which were both linked to the decarbonation of HMCs [40,45,46]. Alternatively, only one peak at around 800 °C, associated with the decarbonation of $CaCO_3$ [41], was observed in the DTG curve of the PC mix, while an extra peak at around 520 °C, corresponding to the decarbonation of HMCs, was evident in the PC + S mix. As the weight loss in these ranges was caused by decarbonation, the CO_2 sequestration of each mix could be calculated accordingly.

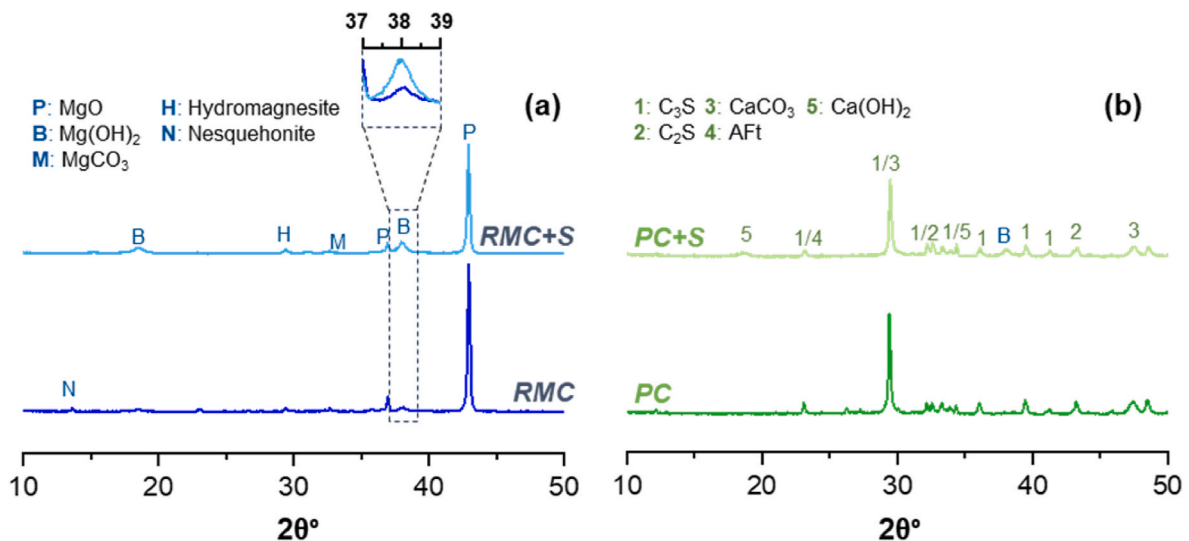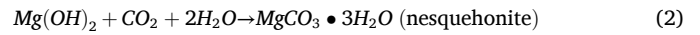Fig. 7 summarised the weight loss at different decomposition stages.

Evidently, due to the incorporation of sludge, the weight loss during the dehydration process was 3.5 % and 2.5 % higher in RMC + S and PC + S mixes, respectively. On the other hand, the incorporation of sludge also increased the CO_2 sequestration of both RMC and PC. Specifically, the sequestrated CO_2 was increased by ~25.9 % and ~41.1 % in RMC and PC mixes, respectively, after 28d of carbonation curing. These substantial increases should be attributed to the ease of the carbonation of main component of sludge, i.e., brucite. As reported in the literature, the carbonation of brucite would directly form different types of hydrated magnesium carbonates (HMCs), such as nesquehonite and hydromagnesite via Equations (2) and (3), respectively [34,47]. Alternatively, the carbonation of RMC and PC could only occur after the formation of hydration products, whilst the hydration of RMC and PC took time, and complete hydration of the binder was barely achievable. Consequently, the incorporation of sludge increased the CO_2 sequestration capability in both PC and RMC systems.

$$Mg(OH)_2 + CO_2 + 2H_2O \rightarrow MgCO_3 \bullet 3H_2O \text{ (nesquehonite)} \tag{2}$$

$$5Mg(OH)_2 + 4CO_2 \rightarrow 4MgCO_3 \bullet Mg(OH)_2 \bullet 4H_2O \text{ (hydromagnesite)} \tag{3}$$

3.5. Chemical composition

The XRD results, presented in Fig. 8, were analyzed to assess the chemical compositions of the carbonated mixes after 28d of curing. Fig. 8 (a) presented the XRD patterns of RMC + S and RMC mixes, revealing MgO as the major compound, as evidenced by the most prominent peak at 42.9° 2θ [48,49]. Furthermore, the intensity of the peak corresponding to brucite at 38.1° 2θ [50] was more pronounced in the RMC + S mix as highlighted in Fig. 8 (a), indicating a higher brucite content. Concerning the carbonation products, hydromagnesite and nesquehonite were identified in the RMC mix, while nesquehonite was absent in the RMC + S mix, though nesquehonite formation was extensively reported in RMC under carbonation curing [3,51,52].

In the PC and PC + S mixes, the predominant chemical composition was $C_3S/CaCO_3$, evident from the most intense peak at around 29.5° 2θ [53]. Other compounds detected by XRD included C_2S, Aft, and $Ca(OH)_2$, aligning with the findings in the literature [54,55]. Notably, brucite was found in the PC + S mix, absent in the PC mix. However, HMCs were not detected in the XRD pattern of PC + S mix. The absence of nesquehonite in the RMC + S mix and HMCs in PC + S mix may be attributed to their minor quantities. Moreover, the newly formed HMCs were reported to show low degree of crystallization at early stage [11,56,57], while the peak intensity in XRD pattern was related to the

Fig. 8. XRD patterns of RMC and PC mixes after 28 days of carbonation curing.
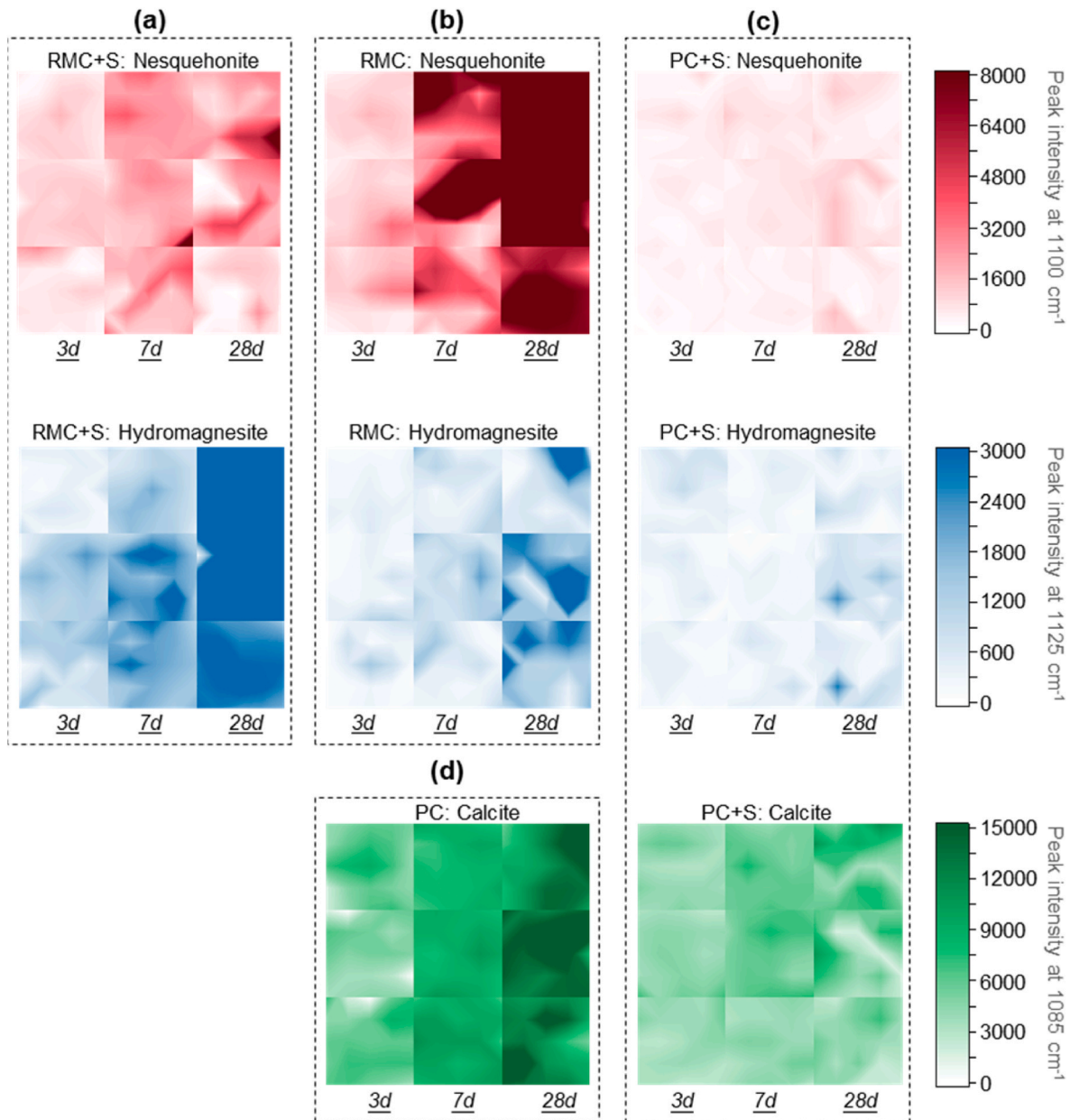
Fig. 9. Raman mapping results of RMC and PC mixes under carbonation curing, showing: (a) RMC + S mix, (b) RMC mix, (c) PC + S mix, and (d) PC mix.

crystallization degree. Therefore, complementary technique, Raman spectroscopy, was employed in present work to further evaluate the carbonated products in these four mixes.

Raman spectroscopy results were presented in Fig. 9. Different colours were associated with the Raman peak intensities at 1085, 1100, and 1125 cm^{-1}, which were corresponding to calcite [58], nesquehonite [59], and hydromagnesite [60], respectively. Fig. 9 (a) showed assessment of carbonation products in RMC + S during carbonation curing, revealing the presence of both nesquehonite and hydromagnesite. An increasing trend for both components was evident by comparing the darkness of the colour. Similar components and trends were observed in the RMC mix, as depicted in Fig. 9 (b). However, it is noteworthy that more nesquehonite was formed in the RMC mix, while more hydromagnesite was found in the RMC + S mix. Therefore, the dominant HMCs formed in RMC + S was hydromagnesite, whilst the major HMCs in RMC was nesquehonite. This observation aligns with the findings reported in the literature [61]. Specifically, the variation in dominant carbonation products can be attributed to the concentration of hydroxyl

ions, which have been shown to facilitate the transformation of nesquehonite into hydromagnesite [62,63]. In this work, the incorporation of sludge, consisting primarily of brucite, naturally elevated the hydroxyl ion concentration, thereby promoting the formation of hydromagnesite.

In addition to nesquehonite and hydromagnesite, calcite was found as one of the carbonation products in PC + S mix as shown in Fig. 9 (c). Notably, due to the formation of calcite (i.e., consumption of CO$_2$ by Ca (OH)$_2$), the amount of nesquehonite and hydromagnesite was reduced by comparing with that in RMC + S mix. Alternatively, only one carbonation product, calcite, was found in the PC mix (Fig. 9 (d)). Considering the linear correlation between the Raman peak intensity and the amount of the carbonated components [58,64], three line plots were presented in Fig. 10 based on the Raman peak intensity to further compare the carbonation products quantitatively. Among all mixes, the highest amount of nesquehonite was formed in RMC mix, while the highest amount of hydromagnesite was found in RMC + S mix. Alternatively, the amount of calcite formed in PC is over two times that in the
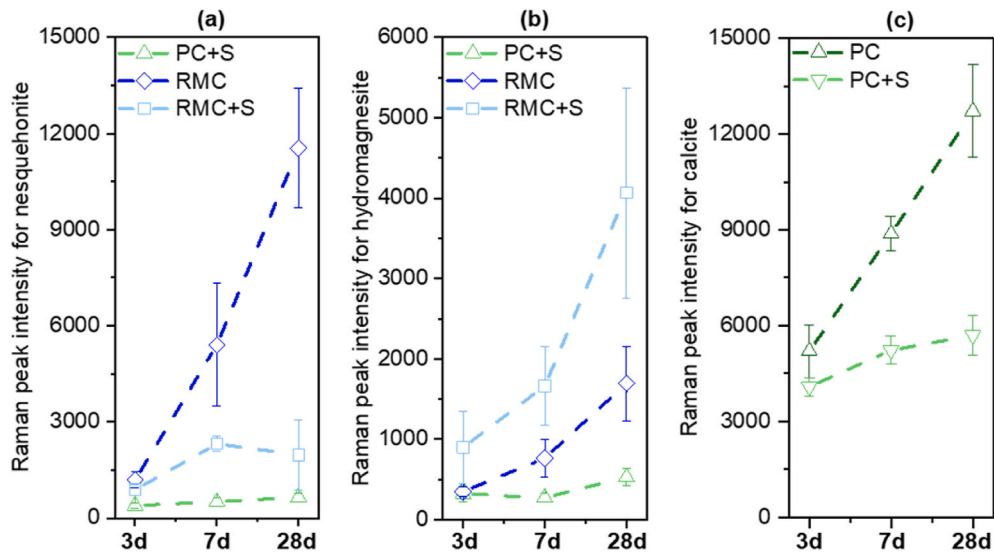
Fig. 10. Line plots of Raman intensity according to the Raman mapping results, showing: Raman peak intensity for (a) nesquehonite, (b) hydromagnesite and (c) calcite.

Table 3
Mass proportions for one cubic meter of the concrete mix used for sustainability analysis.

Mixes (kg/m^3)	Sludge	RMC	PC	Water	Aggregate
RMC + S	542.2	542.2	0.0	0.0	1084.5
RMC	0.0	742.1	0.0	371.1	1113.2
PC + S	531.3	0.0	531.3	0.0	1062.5
PC	0.0	0.0	721.7	360.8	1082.5

Table 4
Inventory data of raw materials used for sustainability analysis [13,65–69].

	Sludge	RMC	PC	Water	Aggregate
CO_2 (kg/kg)	0.04	0.32	0.87	0.19	0.025
Energy (MJ/kg)	0.67	2.96	3.4–5.3[a]	1.2	0.067

[a] The average value was used for calculation.

PC + S mix. The Raman spectroscopy results clearly revealed the coexistence of nesquehonite and hydromagnesite in RMC, RMC + S, and PC + S mixes, with nesquehonite predominant in the RMC mix and hydromagnesite dominant in the RMC + S mix.

3.6. CO_2 emissions and energy consumption

The current investigation aimed to mitigate overall CO_2 emissions and energy consumption associated with the repurposing of reject brine, thereby contributing to the development of a more sustainable concrete mix. Therefore, a comprehensive sustainability analysis was undertaken in this section. Notably, in consideration of the paste nature of the mixes employed in this study, the inclusion of aggregate into the analysis was deemed essential for a more pragmatic assessment. Mass proportions for one cubic meter of concrete were detailed in Table 3, while material sustainability indices for each element were outlined in Table 4 according to the literature [13,65–69]. The resultant CO_2 emissions and energy consumption were depicted in Fig. 11. Apparently, the CO_2 emissions of RMC + S and PC + S were found to be lower than those of RMC and PC, respectively, underscoring the efficacy of sludge incorporation in significantly reducing the CO_2 emissions of both RMC- and PC-based concrete, with reduction rates of ~30 % for both mixes. Furthermore, the inclusion of sludge contributed to a notable reduction in energy consumption by ~25 % for both RMC- and PC-based concrete, as illustrated in Fig. 11 (b). Therefore, the outcomes of the sustainability analysis highlighted the substantial reduction in both CO_2 emissions and energy consumption achieved through the integration of sludge.
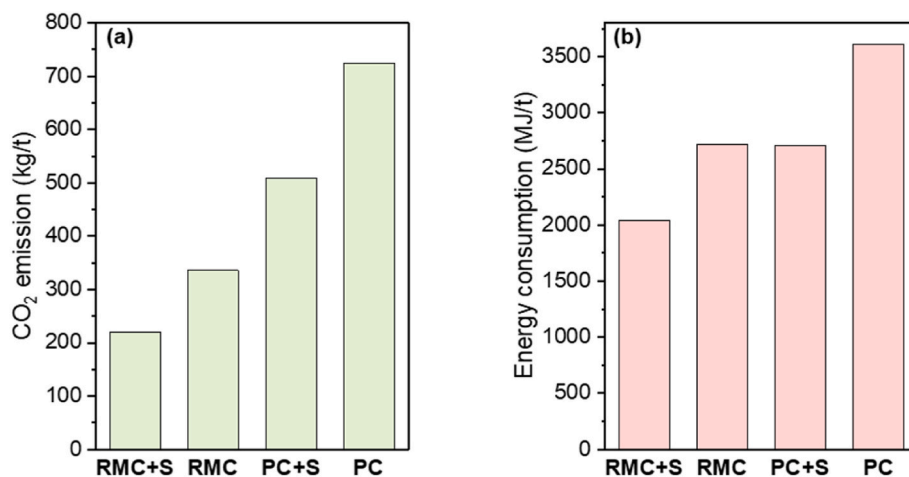

Fig. 11. Sustainability analysis of RMC and PC mixes, indicating: (a) CO_2 emissions and (b) energy consumption.
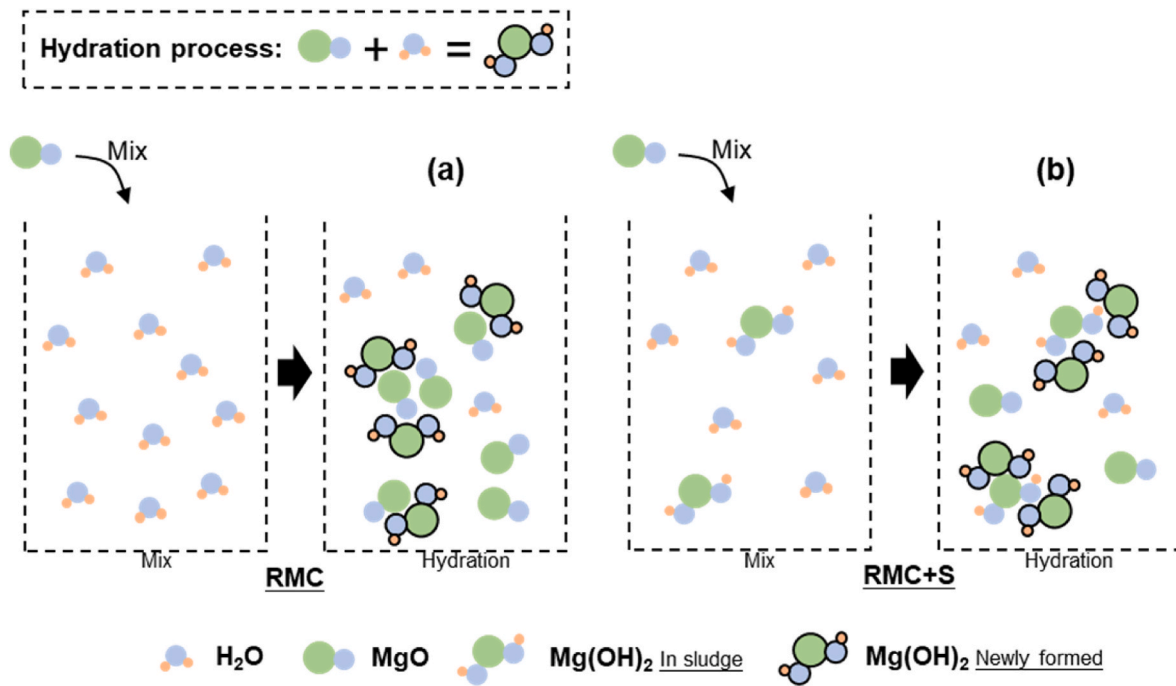
Fig. 12. Schematic representation of the hydration processes in RMC and RMC + S mixes.

4. Discussion

The incorporation of sludge in RMC and PC systems could impact both hydration and carbonation reactions, thereby resulting in diverse performance outcomes. In the RMC system, the effect of sludge on the hydration processes was illustrated in Fig. 12. Upon mixing, MgO reacted with H_2O to form $Mg(OH)_2$ via Equation (4) [70]. Without any alterations, the slow dissolution of MgO and the overall low conversion degree to $Mg(OH)_2$ were attributed to the precipitation of newly formed $Mg(OH)_2$ on the surface of MgO, as depicted in Fig. 12 (a) [71]. Alternatively, in the RMC + S mix, the sludge contained water and brucite at a ratio of 2:1, as depicted in Fig. 12 (b). The existing brucite in the sludge served as a nucleation site for the precipitation of newly formed brucite, leading to a higher hydration rate and degree [34]. Consequently, the amount of newly formed brucite was comparable in RMC and RMC + S mixes, as evidenced by the almost equal hydration heat values reported in Section 3.4. Considering the presence of brucite in sludge, the RMC + S mix thus had a higher total amount of brucite after hydration. This higher brucite content likely contributed to a reduced matrix porosity, aligning with the observed higher strength of RMC + S under ambient conditions in the present work, which was also consistent with similar observations reported in the literature [72]. Additionally, the higher brucite content benefited the formation of HMCs under carbonation curing. Particularly, the formation of hydromagnesite, which is thermodynamically more stable than nesquehonite, was promoted [73]. Given that strength development mainly relies on the changes in the microstructure associated with the formation of HMCs, the RMC + S mix could thereby demonstrate higher strength than the RMC mix.

$$MgO+H_2O\rightarrow Mg(OH)_2 \qquad (4)$$

In the PC system, incorporating sludge also initially enhanced the hydration of PC, as evidenced by the heat release results in Section 3.4. This enhancement could be attributed to the presence of brucite, serving as nucleation sites for the precipitation of CSH gel and portlandite [74]. Consequently, PC and PC + S developed comparable strength in the early stages, as revealed by the 3-day strength results of these two mixes under ambient curing (Fig. 2). However, in the longer term, the PC mix achieved higher strength under ambient conditions due to its higher PC content, and thereby increased hydrate phase formation [75], than that of the PC + S mix. Under carbonation curing, the strength of both PC and PC + S increased due to the formation of carbonation products that densified the microstructures of each matrix [76–78].

According to the sustainability analysis in Section 3.6, the integration of sludge in RMC and PC mixes led to a substantial reduction in both CO_2 emissions and energy consumption. This reduction primarily resulted from the substitution of the original binder with the sludge. Notably, an additional decrease in net CO_2 emissions could be realized by accounting for the CO_2 sequestration capability inherent in all mixes, which is an integral factor often considered in life cycle assessments [7]. According to the TGA results, the CO_2 sequestration capability of mixes containing sludge, namely RMC + S and PC + S, surpassed that of RMC and PC mixes, respectively. The enhanced CO_2 sequestration observed in the RMC mix was attributed to its higher brucite content, a crucial reactant in carbonation reactions [11,47]. It is important to note that the reported CO_2 sequestration of the four mixes pertained to a 28-day carbonation curing period under the conditions used in this study, and this capability may increase with prolonged carbonation duration or adjustment of carbonation conditions. Existing literature indicated that the CO_2 sequestration capability of PC can range between 25 % and 32.5 % by weight, depending on the environmental conditions [79,80]. Alternatively, the CO_2 sequestration capability of brucite was reported to range between 37 wt% and 75 wt% [81,82]. Consequently, a substantial reduction in net CO_2 emissions could be achieved by deducting the sequestered CO_2, especially for the RMC + S and PC + S mixes.

5. Conclusion

This work assessed the viability of a two-step method to reuse reject brine to enhance the sustainability of PC- and RMC-based mixes. Specifically, the sludge generated through the precipitation and filtration steps involved during the synthesis of RMC from reject brine was directly used as a supplementary cementitious material in RMC and PC mixes. The resulting reaction mechanisms, mechanical performance and microstructural development were thoroughly evaluated to obtain the following key findings.

- The inclusion of sludge led to an increase in the strength of RMC under both ambient and carbonation curing conditions, surpassing a two-fold increase under the latter condition. Conversely, a reduction in strength was observed in PC mixes containing sludge. However, the strength still exceeded 30 MPa under carbonation curing. The observed variations in the mechanical performance of RMC and PC mixes with the use of sludge were strongly correlated with the pore size distribution of each mix.

- The hydration heat of PC and RMC mixes exhibited accelerated rates at early stages in the presence of sludge, owing to the nucleation sites provided by the brucite in the sludge. Nevertheless, the ultimate heat release was comparable in RMC and lower in PC mixes.

- The predominant carbonation product in the RMC mix was nesquehonite, which transformed into hydromagnesite with the incorporation of sludge. In the PC mix, the inclusion of sludge resulted in the formation of both nesquehonite and hydromagnesite, while the main carbonation product remained calcite.

- The inclusion of sludge exhibited a marked enhancement in the CO_2 sequestration capacity for both RMC and PC mixes, demonstrating increases in the amount of CO_2 sequestered at 28 days by ~25.9 % and ~41.1 %, respectively. The integration of sludge itself (i.e. without relying on carbonation) also resulted in a notable ~30 % reduction in CO_2 emissions and a ~25 % decrease in energy consumption for both RMC and PC mixes.

Overall, the outcomes of this work validate the feasibility of utilizing sludge in RMC and PC mixes, presenting an innovative method for reusing reject brine with a significantly reduced environmental impact. As future perspectives, further research could explore optimization strategies and large-scale applications to facilitate the seamless integration of this innovative method into sustainable construction practices.

CRediT authorship contribution statement

Tangwei Mi: Writing – review & editing, Writing – original draft, Methodology, Investigation, Formal analysis, Data curation, Conceptualization. **Yongqiang Li:** Writing – review & editing, Writing – original draft, Investigation, Formal analysis. **En-Hua Yang:** Writing – review & editing, Writing – original draft, Supervision, Resources, Project administration, Methodology, Funding acquisition, Conceptualization. **Cise Unluer:** Writing – review & editing, Writing – original draft, Supervision, Resources, Project administration, Funding acquisition, Conceptualization.

Declaration of competing interest

None

Acknowledgements

Data availability

No data was used for the research described in the article.

References

[1] R. Hay, K. Celik, Accelerated carbonation of reactive magnesium oxide cement (RMC)-based composite with supercritical carbon dioxide (scCO2), J. Clean. Prod. 248 (2020) 119282.

[2] S. Ruan, E.-H. Yang, C. Unluer, Production of reactive magnesia from desalination reject brine and its use as a binder, J. CO2 Util. 44 (2021) 101383.

[3] C. Unluer, A. Al-Tabbaa, Impact of hydrated magnesium carbonate additives on the carbonation of reactive MgO cements, Cement Concr. Res. 54 (2013) 87–97.

[4] H. Dong, C. Unluer, E.-H. Yang, A. Al-Tabbaa, Synthesis of reactive MgO from reject brine via the addition of NH4OH, Hydrometallurgy 169 (2017) 165–172.

[5] H. Dong, C. Unluer, E.-H. Yang, F. Jin, A. Al-Tabbaa, Microstructure and carbon storage capacity of hydrated magnesium carbonates synthesized from different sources and conditions, J. CO2 Util. 34 (2019) 353–361.

[6] H. Dong, C. Unluer, E.-H. Yang, A. Al-Tabbaa, Recovery of reactive MgO from reject brine via the addition of NaOH, Desalination 429 (2018) 88–95.

[7] S. Ruan, C. Unluer, Comparative life cycle assessment of reactive MgO and Portland cement production, J. Clean. Prod. 137 (2016) 258–273.

[8] C. Unluer, A. Al-Tabbaa, Enhancing the carbonation of MgO cement porous blocks through improved curing conditions, Cement Concr. Res. 59 (2014) 55–65.

[9] A.M.O. Mohamed, M. Maraqa, J. Al Handhaly, Impact of land disposal of reject brine from desalination plants on soil and groundwater, Desalination 182 (2005) 411–433.

[10] E. Jones, M. Qadir, M.T.H. van Vliet, V. Smakhtin, S.-m. Kang, The state of desalination and brine production: a global outlook, Sci. Total Environ. 657 (2019) 1343–1356.

[11] I. Singh, R. Hay, K. Celik, Recovery and direct carbonation of brucite from desalination reject brine for use as a construction material, Cement Concr. Res. 152 (2022) 106673.

[12] H. Dong, E.-H. Yang, C. Unluer, F. Jin, A. Al-Tabbaa, Investigation of the properties of MgO recovered from reject brine obtained from desalination plants, J. Clean. Prod. 196 (2018) 100–108.

[13] F. Shahbaz, I. Singh, P. Krishnan, K. Celik, Life cycle assessment of brucite and synthetic MgO produced from reject brine using different alkalis, J. Clean. Prod. 380 (2022) 135071.

[14] M. Turek, W. Gnot, Precipitation of magnesium hydroxide from brine, Ind. Eng. Chem. Res. 34 (1995) 244–250.

[15] N. Petric, V. Martinac, M. Labor, The effect of mannitol and pH of the solution on the properties of sintered magnesium oxide obtained from sea water, Chem. Eng. Technol.: Industrial Chemistry-Plant Equipment-Process Engineering-Biotechnology 20 (1997) 36–39.

[16] M.H. El-Naas, Reject Brine Management, Desalination, Trends and Technologies, 2011, pp. 237–252.

[17] K.T. Tran, K.S. Han, S.J. Kim, M.J. Kim, T. Tran, Recovery of magnesium from Uyuni salar brine as hydrated magnesium carbonate, Hydrometallurgy 160 (2016) 106–114.

[18] S.H. Chu, E.H. Yang, C. Unluer, Chemical synthesis of magnesium oxide (MgO) from brine towards minimal energy consumption, Desalination 556 (2023) 116594.

[19] S.-C. Kou, B.-J. Zhan, C.-S. Poon, Properties of partition wall blocks prepared with fresh concrete wastes, Constr. Build. Mater. 36 (2012) 566–571.

[20] S.-c. Kou, B.-j. Zhan, C.-s. Poon, Feasibility study of using recycled fresh concrete waste as coarse aggregates in concrete, Constr. Build. Mater. 28 (2012) 549–556.

[21] J. Zhang, T. Fujiwara, Concrete sludge powder for soil stabilization, Transp. Res. Rec. 2026 (2007) 54–59.

[22] M. Zervaki, C. Leptokaridis, S. Tsimas, Reuse of by-products from ready-mixed concrete plants for the production of cement mortars, Journal of sustainable development of energy, water and environment systems 1 (2013) 152–162.

[23] D. Xuan, B. Zhan, C.S. Poon, W. Zheng, Innovative reuse of concrete slurry waste from ready-mixed concrete plants in construction products, J. Hazard Mater. 312 (2016) 65–72.

[24] L. Liu, Z. He, X. Cai, S. Fu, Application of low-field NMR to the pore structure of concrete, Appl. Magn. Reson. 52 (2021) 15–31.

[25] J. Zhang, J. Guo, D. Li, Y. Zhang, F. Bian, Z. Fang, The influence of admixture on chloride time-varying diffusivity and microstructure of concrete by low-field NMR, Ocean. Eng. 142 (2017) 94–101.

[26] W. Liu, H. Du, P. Yi, Y. Li, Y. Luo, Q. Chen, F. Xing, The early hydration and rheological characteristics of cement paste containing co-combustion fly ash, J. Build. Eng. 78 (2023) 107736.

[27] F. Jin, A. Al-Tabbaa, Strength and hydration products of reactive MgO–silica pastes, Cement Concr. Compos. 52 (2014) 27–33.

[28] R.-M. Pellenq, N. Lequeux, H. Van Damme, Engineering the bonding scheme in C–S–H: the iono-covalent framework, Cement Concr. Res. 38 (2008) 159–174.

[29] R. Hay, B. Peng, K. Celik, Filler effects of CaCO3 polymorphs derived from limestone and seashell on hydration and carbonation of reactive magnesium oxide (MgO) cement (RMC), Cement Concr. Res. 164 (2023) 107040.

[30] N.T. Dung, C. Unluer, Improving the performance of reactive MgO cement-based concrete mixes, Constr. Build. Mater. 126 (2016) 747–758.

[31] P. Hewlett, Lea's Chemistry of Cement and Concrete fifth ed., Elsevier Science2019.

[32] A.J.N. MacLeod, F.G. Collins, W. Duan, Effects of carbon nanotubes on the early-age hydration kinetics of Portland cement using isothermal calorimetry, Cement Concr. Compos. 119 (2021) 103994.

[33] Z. Li, D. Lu, X. Gao, Analysis of correlation between hydration heat release and compressive strength for blended cement pastes, Constr. Build. Mater. 260 (2020) 120436.

[34] N.T. Dung, C. Unluer, Development of MgO concrete with enhanced hydration and carbonation mechanisms, Cement Concr. Res. 103 (2018) 160–169.

[35] Y. Li, H. Ma, H. Wen, J. Yuan, Y. Zhang, Y. Li, H. Zhou, J. Chen, Influence of pore size distribution on concrete cracking with different AEA content and curing age using acoustic emission and low-field NMR, J. Build. Eng. 58 (2022) 105059.

[36] D. Li, D. Niu, Q. Fu, D. Luo, Fractal characteristics of pore structure of hybrid Basalt–Polypropylene fibre-reinforced concrete, Cement Concr. Compos. 109 (2020) 103555.

[37] R. Kumar, B. Bhattacharjee, Porosity, pore size distribution and in situ strength of concrete, Cement Concr. Res. 33 (2003) 155–164.

[38] B. Šavija, M. Luković, Carbonation of cement paste: understanding, challenges, and opportunities, Constr. Build. Mater. 117 (2016) 285–301.

[39] N.T. Dung, A. Lesimple, R. Hay, K. Celik, C. Unluer, Formation of carbonate phases and their effect on the performance of reactive MgO cement formulations, Cement Concr. Res. 125 (2019) 105894.

[40] R.L. Frost, S. Bahfenne, J. Graham, W.N. Martens, Thermal stability of artinite, dypingite and brugnatellite—implications for the geosequestration of green house gases, Thermochim. Acta 475 (2008) 39–43.

[41] B. Lu, C. Shi, J. Zhang, J. Wang, Effects of carbonated hardened cement paste powder on hydration and microstructure of Portland cement, Constr. Build. Mater. 186 (2018) 699–708.

[42] P. Ballirano, C. De Vito, V. Ferrini, S. Mignardi, The Thermal Behaviour and Structural Stability of Nesquehonite, MgCO3·3H2O, Evaluated by in Situ Laboratory Parallel-Beam X-Ray Powder Diffraction: New Constraints on CO2 Sequestration within Minerals, J. Hazard Mater vol. 178 (2010) 522–528.

[43] J. Ren, B. Liu, J. Guo, J. Liu, F. Xing, H. Zhu, L. Zhao, T. Mi, Bio-treatment of municipal solid waste incineration fly ash: a sustainable path for recyclability, J. Clean. Prod. (2023) 139869.

[44] G. Villain, M. Thiery, G. Platret, Measurement methods of carbonation profiles in concrete: Thermogravimetry, chemical analysis and gammadensimetry, Cement Concr. Res. 37 (2007) 1182–1192.

[45] L. Wang, L. Chen, J.L. Provis, D.C.W. Tsang, C.S. Poon, Accelerated carbonation of reactive MgO and Portland cement blends under flowing CO2 gas, Cement Concr. Compos. 106 (2020) 103489.

[46] N.T. Dung, C. Unluer, Sequestration of CO2 in reactive MgO cement-based mixes with enhanced hydration mechanisms, Constr. Build. Mater. 143 (2017) 71–82.

[47] T. Mi, E.-H. Yang, C. Unluer, Investigation of the properties of reactive MgO-based cements and their effect on performance, Cement Concr. Compos. 138 (2023) 104984.

[48] C. Pischetola, F. Hesse, J.-W.G. Bos, F. Cárdenas-Lizana, Effect of Lewis basicity on the continuous gas phase condensation of benzaldehyde with acetophenone over MgO, Appl. Catal. Gen. 623 (2021) 118277.

[49] Y.H. Taufiq-Yap, H.V. Lee, M.Z. Hussein, R. Yunus, Calcium-based mixed oxide catalysts for methanolysis of Jatropha curcas oil to biodiesel, Biomass Bioenergy 35 (2011) 827–834.

[50] J.A. Wang, O. Novaro, X. Bokhimi, T. López, R. Gómez, J. Navarrete, M.E. Llanos, E. López-Salinas, Characterizations of the thermal decomposition of brucite prepared by sol–gel technique for synthesis of nanocrystalline MgO, Mater. Lett. 35 (1998) 317–323.

[51] R. Hay, C. Otchere, G. Kashwani, K. Celik, Recycling carbonated reactive magnesium cement (RMC) as a building material, J. Clean. Prod. 320 (2021) 128838.

[52] N.T. Dung, R. Hay, A. Lesimple, K. Celik, C. Unluer, Influence of CO2 concentration on the performance of MgO cement mixes, Cement Concr. Compos. 115 (2021) 103826.

[53] V. Rostami, Y. Shao, A.J. Boyd, Durability of concrete pipes subjected to combined steam and carbonation curing, Constr. Build. Mater. 25 (2011) 3345–3355.

[54] V. Rostami, Y. Shao, A.J. Boyd, Z. He, Microstructure of cement paste subject to early carbonation curing, Cement Concr. Res. 42 (2012) 186–193.

[55] Z. Yu, Y. Meng, K.H. Mo, H. Liu, T.-C. Ling, Influences of w/c and CO2 curing duration on the high temperature properties of cement pastes, J. Build. Eng. 69 (2023) 106293.

[56] R. Hao, Investigation into the Production of Carbonates and Oxides from Synthetic Brine through Carbon Sequestration, Department of Engineering, University of, Cambridge, 2017.

[57] A. Jarosinski, L. MadeJSKA, MgCO3 obtaining from wastewaters generated during the acidic leaching of zinc concentrates, Miner. Slov. 42 (2010) 317–320.

[58] T. Mi, Y. Li, W. Liu, W. Li, W. Long, Z. Dong, Q. Gong, F. Xing, Y. Wang, Quantitative evaluation of cement paste carbonation using Raman spectroscopy, npj Mater. Degrad. 5 (2021) 35.

[59] M.C. Hales, R.L. Frost, W.N. Martens, Thermo-Raman spectroscopy of synthetic nesquehonite—implication for the geosequestration of greenhouse gases, J. Raman Spectrosc. 39 (2008) 1141–1149.

[60] R.L. Frost, Raman spectroscopic study of the magnesium carbonate mineral hydromagnesite (Mg5 [(CO3) 4 (OH) 2]· 4H2O), J. Raman Spectrosc. 42 (2011) 1690–1694.

[61] T. Mi, X. Chen, E.-H. Yang, C. Unluer, Quantification of carbonated Mg-based cement pastes by Raman spectroscopy, Cement Concr. Res. 178 (2024) 107454.

[62] Z. Zhang, Y. Zheng, Y. Ni, Z. Liu, J. Chen, X. Liang, Temperature-and pH-dependent morphology and FT– IR analysis of magnesium carbonate hydrates, J. Phys. Chem. B 110 (2006) 12969–12973.

[63] L. Hopkinson, P. Kristova, K. Rutt, G. Cressey, Phase transitions in the system MgO–CO2–H2O during CO2 degassing of Mg-bearing solutions, Geochem. Cosmochim. Acta 76 (2012) 1–13.

[64] P. Nie, T. Dong, S. Xiao, L. Lin, Y. He, F. Qu, Quantitative determination of thiabendazole in soil extracts by surface-enhanced Raman spectroscopy, Molecules 23 (2018) 1949.

[65] W.-C. Choi, H.-D. Yun, J.-W. Kang, S.-W. Kim, Development of recycled strain-hardening cement-based composite (SHCC) for sustainable infrastructures, Compos. B Eng. 43 (2012) 627–635.

[66] G.A. Keoleian, A. Kendall, J.E. Dettling, V.M. Smith, R.F. Chandler, M.D. Lepech, V. C. Li, Life cycle modeling of concrete bridge design: comparison of engineered cementitious composite link slabs and conventional steel expansion joints, J. Infrastruct. Syst. 11 (2005) 51–60.

[67] J. Yu, K.Y. Leung, Strength Improvement of Strain-Hardening Cementitious Composites with Ultrahigh-Volume Fly Ash, J. Mater. Civ. Eng vol. 29 (2017) 05017003.

[68] D. Kumar, T. Mi, E.-H. Yang, Improving the material sustainability of strain-hardening magnesium-silicate-hydrate composite by incorporating aggregates, Constr. Build. Mater. 407 (2023) 133576.

[69] N. Sahoo, A. Kumar, Samsher, Review on energy conservation and emission reduction approaches for cement industry, Environmental Development 44 (2022) 100767.

[70] J.J. Thomas, S. Musso, I. Prestini, Kinetics and activation energy of magnesium oxide hydration, J. Am. Ceram. Soc. 97 (2014) 275–282.

[71] O. Fruhwirth, G.W. Herzog, I. Hollerer, A. Rachetti, Dissolution and hydration kinetics of MgO, Surf. Technol. 24 (1985) 301–317.

[72] Z. Li, J. Qian, J. Qin, Y. Hua, Y. Yue, H. Tang, Cementitious and hardening properties of magnesia (MgO) under ambient curing conditions, Cement Concr. Res. 170 (2023) 107184.

[73] R.A. Robie, B.S. Hemingway, The enthalpies of formation of nesquehonite, MgCO3· 3H2O, and hydromagnesite, 5MgO· 4CO2· 5H2O, J. Res. U. S. Geol. Surv. 1 (1973) 543–547.

[74] E. John, T. Matschei, D. Stephan, Nucleation seeding with calcium silicate hydrate – a review, Cement Concr. Res. 113 (2018) 74–85.

[75] Z. Zhang, Y. Yan, Z. Qu, G. Geng, Endowing strength to calcium silicate hydrate (C-S-H) powder by high pressure mechanical compaction, Cement Concr. Res. 159 (2022) 106858.

[76] B.J. Zhan, D.X. Xuan, C.S. Poon, C.J. Shi, Mechanism for rapid hardening of cement pastes under coupled CO2-water curing regime, Cement Concr. Compos. 97 (2019) 78–88.

[77] A. Neves Junior, R.D. Toledo Filho, E. de Moraes Rego Fairbairn, J. Dweck, The effects of the early carbonation curing on the mechanical and porosity properties of high initial strength Portland cement pastes, Constr. Build. Mater. 77 (2015) 448–454.

[78] M. Zajac, L. Irbe, F. Bullerjahn, H. Hilbig, M. Ben Haha, Mechanisms of carbonation hydration hardening in Portland cements, Cement Concr. Res. 152 (2022) 106687.

[79] A. Arrigoni, R. Pelosato, P. Melià, G. Ruggieri, S. Sabbadini, G. Dotelli, Life cycle assessment of natural building materials: the role of carbonation, mixture components and transport in the environmental impacts of hempcrete blocks, J. Clean. Prod. 149 (2017) 1051–1061.

[80] L. Haselbach, A. Alam, Carbon Sequestration in Old and New Portland Cement Concrete Pavement Interiors, Innovative Materials and Design for Sustainable Transportation Infrastructure2015, pp. 71-82.

[81] K. Rausis, A. Ćwik, I. Casanova, Phase evolution during accelerated CO2 mineralization of brucite under concentrated CO2 and simulated flue gas conditions, J. CO2 Util. 37 (2020) 122–133.

[82] A.L. Harrison, I.M. Power, G.M. Dipple, Accelerated carbonation of brucite in mine tailings for carbon sequestration, Environ. Sci. Technol. 47 (2013) 126–134.